



Enhancing antifogging/frost-resisting performances of amphiphilic coatings via cationic, zwitterionic or anionic polyelectrolytes



Shan Bai^a, Xiaohui Li^{a,*}, Rongchun Zhang^b, Chuan Li^a, Kongying Zhu^a, Pingchuan Sun^b, Yunhui Zhao^a, Lixia Ren^a, Xiaoyan Yuan^{a,*}

^a School of Materials Science and Engineering, and Tianjin Key Laboratory of Composite and Functional Materials, Tianjin University, Tianjin 300350, China

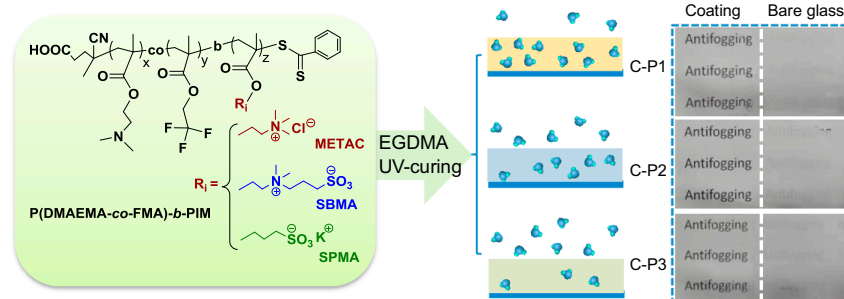
^b State Key Laboratory of Medicinal Chemical Biology, Nankai University, Tianjin 300071, China

HIGHLIGHTS

- P(DMAEMA-co-FMA)-*b*-polyelectrolytes were synthesized via RAFT polymerization.
- Amphiphilic coatings were developed from the copolymers with EGDMA via UV-curing.
- The prepared coatings exhibited enhanced antifogging and frost-resisting properties.
- The cationic and zwitterionic coatings exhibited superior antifogging properties.
- The anionic polyelectrolyte-based coating demonstrated a better frost-resisting behavior.

GRAPHICAL ABSTRACT

Amphiphilic coatings containing cationic, zwitterionic or anionic polyelectrolytes exhibited enhanced antifogging and frost-resisting properties.



ARTICLE INFO

Keywords:
Copolymer
Polyelectrolyte
Amphiphilic coating
Antifogging
Frost-resisting

ABSTRACT

Polymeric antifogging and frost-resisting coatings were successfully prepared, but the performances of amphiphilic coatings containing different kinds of cationic, zwitterionic and anionic polyelectrolytes are still needed to investigate systematically. In this work, antifogging/frost-resisting coatings with high transparency were developed from amphiphilic copolymers of cationic, zwitterionic or anionic poly(2-(dimethylamino)ethyl methacrylate (DMAEMA)-co-2,2,2-trifluoroethyl methacrylate (FMA))-*b*-polyelectrolytes with a small amount of ethylene glycol dimethacrylate via UV-curing. Studies on the prepared amphiphilic coatings suggested that the cationic and zwitterionic coatings exhibited superior antifogging properties, whereas the anionic polyelectrolyte-based coating demonstrated a better frost-resisting behavior. Water molecule activities in the amphiphilic coatings were analyzed by differential scanning calorimetry, Raman spectroscopy and low field nuclear magnetic resonance. It was found that the cationic and zwitterionic coatings containing 2-(methacryloyloxy)-ethyltrimethyl ammonium chloride and sulfobetaine methacrylate, respectively, exhibited stronger polymer-water interactions dominated by strong hydrogen bonds, and held more nonfreezable water content with shorter transverse spin-spin relaxation time T_2 than the anionic coating containing 3-sulfopropyl methacrylate potassium (SPMA). Electrostatic interactions between anionic SPMA and DMAEMA units in the copolymer could weaken the polymer-water interaction, leading to a compromise in the antifogging performance and an enhancement of frost-resisting ability of the coating. The results of this study would be applicable for exploring the advanced antifogging/frost-resisting coatings.

* Corresponding authors.

E-mail addresses: lixiaohui@tju.edu.cn (X. Li), yuanxy@tju.edu.cn (X. Yuan).

1. Introduction

Fogging phenomena caused by water droplet condensation owing to temporary changes in temperature and humidity could lead to much inconvenience and even danger in our daily life. Fog formed on solar energy arrays, analytical and medical instruments, as well as other display devices could dramatically decrease their optical efficiency [1,2]. To mitigate the fogging problem, various surfaces have been developed based on bioinspired materials with superhydrophilicity or superhydrophobicity [1,3–6]. However, the preparation of super-wettable surfaces with complicated textures still remained technologically challenging. In addition, the micro/nano-structures on the surfaces are susceptible for the long-term use [1,7–10].

In recent years, remarkable antifogging performances were achieved by water-absorbed coatings with amphiphilicity [11–20]. For instance, Ming *et al.* developed an acrylate random copolymer coating comprising 2-(dimethylamino)ethyl methacrylate (DMAEMA) and methyl methacrylate (MMA), which exhibited excellent antifogging behaviors due to the hydrophilicity/hydrophobicity balance regulated by DMAEMA and MMA [12–14]. Taking the synergistic advantage of hygroscopicity and hydrophobicity, a zwitter-wettable antifogging film consisting of water-absorbable chitosan/carboxymethyl cellulose capped with a hydrophobic Nafion layer was successfully prepared via layer-by-layer assembly [15].

Different from fog formation, frost usually generated when the temperature was below both the freezing point of water and the dew point of the surrounding environment, which could also arouse concerns of energy consumption and safety [20–23]. Cohen and co-workers demonstrated that the frost-resisting performance could be greatly improved by addition of poly(ethylene glycol) (PEG) to the multilayer film, because PEG provided an additional capacity to force water molecules to disperse in the coatings as nonfreezable water [20]. The existence of nonfreezable water in the coatings played an important role in preventing fog or frost formation via molecular interactions with polymers [19,20].

Polyelectrolytes, such as poly(ethylenimine), poly(acrylic acid), PDMAEMA with quaternary ammonium and poly(sulfobetaine)

(methacrylate) (PSBMA) have ever been studied in preparation of antifogging, frost-resisting, and anti-icing coatings [11,13,19,24–30]. The study on the anti-icing mechanism of polyelectrolyte brushes and the counterions suggested that the ice propagation rate could increase up to three orders of magnitude by changing the ionic pairs of the outmost polyelectrolyte layer [28]. It was assumed that the polyelectrolyte types could affect their interactions with water molecules, and thus further improve the antifogging/frost-resisting performances of the prepared coatings.

Amphiphilic antifogging/anti-icing coatings containing zwitterionic units were prepared in our previous reports, and it was found that the hydrophilic component could absorb water molecules via polymer-water interactions and the hydrophobic counterpart could prevent excessive water from entering into coatings [19,30]. Followed by these studies, further investigations are necessary to examine the effect of different polyelectrolytes on the polymer-water interactions and the enhanced antifogging/frost-resisting performances. In this study, amphiphilic antifogging/frost-resisting coatings were developed with three different kinds of copolymers containing cationic 2-(methacryloyloxy)-ethyltrimethylammonium chloride (METAC), zwitterionic SBMA or anionic 3-sulfopropyl methacrylate potassium (SPMA). Poly(2-(dimethylamino)ethyl methacrylate-co-2,2,2-trifluoroethyl methacrylate)-*b*-polyelectrolytes (P(DMAEMA-co-FMA)-*b*-polyelectrolytes) were synthesized via reversible addition-fragmentation chain transfer (RAFT) polymerization. Then, the coatings were prepared by adding a certain amount of ethylene glycol dimethacrylate (EGDMA) to form a semi-interpenetrating polymer network (SIPN) via UV-curing to ensure the coating stability and durability [12]. It was hypothesized that the antifogging/frost-resisting performances of the amphiphilic coatings containing polyelectrolytes could be attributed to the strong polymer-water interactions. Therefore, the antifogging/frost-resisting properties of the prepared polyelectrolyte-based coatings were studied systematically by further quantitative analyses of the polymer-water interactions via differential scanning calorimetry (DSC), Raman spectroscopy and low field nuclear magnetic resonance (LF NMR).

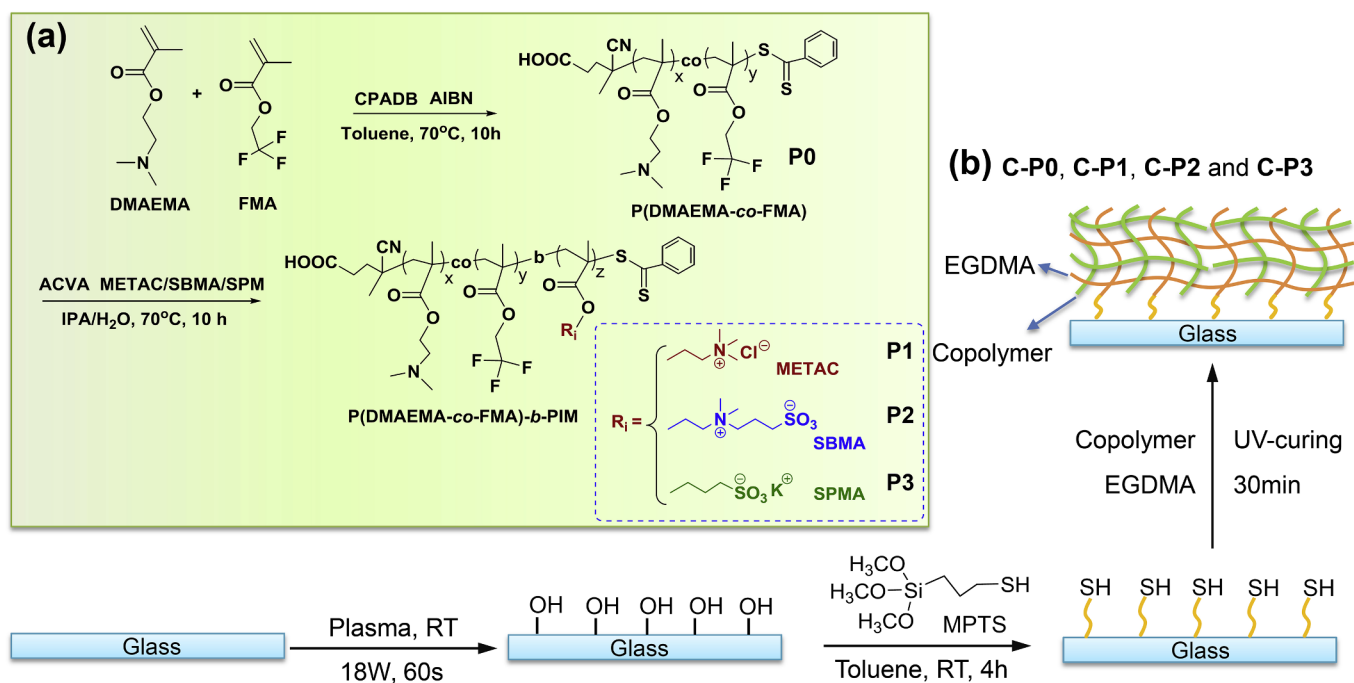


Fig. 1. Synthesis of P(DMAEMA-co-FMA)-*b*-PIM copolymers containing cationic METAC, zwitterionic SBMA and anionic SPMA units, respectively (a) and schematic preparation of the polyelectrolyte-based coatings (b).

2. Material and methods

2.1. Synthesis of P(DMAEMA-co-FMA)-b-polyelectrolytes

As shown in Fig. 1(a), three kinds of P(DMAEMA-co-2,2,2-trifluoroethyl methacrylate)-b-polyelectrolyte copolymers (P(DMAEMA-co-FMA)-b-PIM) containing different ionic monomers (IMs) of cationic METAC, zwitterionic SBMA and anionic SPMA, respectively, were synthesized via RAFT polymerization. Firstly, P(DMAEMA-co-FMA) with a 150/20 feeding ratio of DMAEMA and FMA was synthesized, and subsequently the P(DMAEMA-co-FMA)-b-PIM polyelectrolyte-based copolymers were prepared by using P(DMAEMA-co-FMA) as the polymeric chain transfer agent with feeding ratio of DMAEMA to IM as 150/30. The detailed synthesis procedure has been given in the [Supplementary Material](#). For convenience, the P(DMAEMA-co-FMA) copolymer is abbreviated as **P0**, and the three P(DMAEMA-co-FMA)-b-PIM copolymers with different IMs, i.e., cationic P(DMAEMA-co-FMA)-b-PMETAC, zwitterionic P(DMAEMA-co-FMA)-b-PSBMA and anionic P(DMAEMA-co-FMA)-b-PSPMA are denoted as **P1**, **P2** and **P3**, respectively.

Compositions and molecular weight of the prepared copolymers are shown in [Table 1](#). Characterizations of the prepared copolymers performed by proton nuclear magnetic resonance (^1H NMR) spectroscopy, gel permeation chromatography (GPC) and Fourier transform infrared spectroscopy (FTIR) are given in [Figs. S1–S3](#), respectively. All of the results verified the chemical structure of the synthesized copolymers, and similar compositions of DMAEMA, FMA and IM in **P1**, **P2** and **P3** copolymers were obtained, ensuring the suitable comparison in anti-fogging/frost-resisting performances of three kinds of polyelectrolyte-based coatings. The copolymer morphology was observed by a transmission electron microscope (TEM) at room temperature at 100 kV and an atomic force microscope (AFM) as shown in [Fig. S4](#).

2.2. Preparation of the polyelectrolyte-based coatings

The coatings were prepared from the P(DMAEMA-co-FMA)-b-PIM polyelectrolyte-based copolymers on the glass substrates with a certain amount of EGDMA via UV-curing as shown in [Fig. 1\(b\)](#). Firstly, glass slides ($2.54 \times 7.62 \text{ cm}^2$) were treated by plasma (18 W, 60 s) to produce hydroxyl groups on their surfaces, and then immersed in a 5% (v/v) solution of (3-mercaptopropyl)trimethoxysilane (MPTS) in toluene at room temperature for 4 h to generate -SH groups. After that, the MPTS-modified glass slides were sonicated consecutively in toluene, toluene/ethanol mixture (50%, v/v) and ethanol for 5 min and followed by rinsing with ethanol and blow-drying with air [\[31\]](#). A determined amount of the copolymers (**P0**, **P1**, **P2** or **P3**) were dissolved in 2,2,2-trifluoroethanol to obtain a 50 mg/mL copolymer solution. EGDMA (10 wt% relative to the copolymer) and benzoin dimethyl ether (20 wt % with respect to EGDMA) were also added to the homogeneous

solutions. The polyelectrolyte-based coatings were prepared by dripping the solutions onto both halves of MPTS-modified glass slides and curing under UV irradiation (365 nm, 125 W) for 30 min. The resulting SIPN coatings containing copolymers **P0**, **P1**, **P2** and **P3** were obtained by further drying in a vacuum oven at 60 °C for 2 h, and denoted as **C-P0**, **C-P1**, **C-P2** and **C-P3**, respectively. The thickness of the obtained coatings was typically about 8 μm determined by the NT220 Coating Thickness Measurer (Beijing Timesun Science & Trade Co. Ltd., China).

2.3. Characterizations

Surface compositions of the coatings were detected by X-ray photoelectron spectroscopy (XPS, PHI 5000C ECSA, Perkin-Elmer, USA) with Al K α radiation source under a pressure of about 6.7×10^{-6} Pa. Instead of glass slides, the coatings were cast onto the aluminum sheet, and then vacuumized over night before the XPS measurement. Attenuated total reflectance-Fourier transform infrared spectroscopy (ATR-FTIR) (TENSO 27 spectrometer, German) was used to characterize the surface chemical structure of the prepared coatings, which were scraped from glass slides gingerly, and the surface morphology of the prepared coatings was detected by AFM (CSPM5500A, Benyuan Nano-Instruments Ltd., China) and scanning electron microscope (SEM) (Hitachi SU1510, Japan) at room temperature. Water contact angles (WCA) of the prepared coatings and their evolution with time were measured at room temperature with a 5 μL deionized water drops by using a JC 2000D CA meter (Shanghai Zhongchen Instrument Co. Ltd., China). Each coating was tested in five parallels. According to Owens-Wendt-Kaelble (OWK) method [\[32\]](#), the surface energy of the polyelectrolyte-based coatings was measured and calculated by the JC 2000D software. Deionized water and *n*-hexadecane were used as the test liquids respectively. Both water and *n*-hexadecane contact angles were used by the initial value.

Antifogging performances were tested by using both the hot-vapor and cold-warm methods [\[19\]](#). For the hot-vapor method, the half-coated glass substrate was held 3 cm above hot water (~ 80 °C) for 15 s and photographed. Cold-warm method was performed by placing the sample in refrigerator (-20 °C) for 30 min and subsequently exposed to laboratory environment (~ 15 °C, 40% RH), photographed immediately. The transmittance values ranging from 400 to 800 nm of the prepared coatings on the glass substrates were recorded by a 722 s visible spectrophotometer (Shanghai Jinghua Technology Instruments Co. Ltd., China). Frost-resisting performance was evaluated according to the reference [\[21\]](#). In brief, all the prepared coatings on glass slides ($1 \times 1 \text{ cm}^2$) were placed on a custom-made cooling stage at room temperature and RH of 50%. The samples on the stage were cooled from room temperature to -5 °C at a rate of 2 °C/min and then maintained at -5 °C during the test. Optical images were taken every 1 min when the stage temperature reached -5 °C to observe the frost-resisting performance. The water stability of the prepared coatings was measured and

Table 1
Compositions and molecular weights of P(DMAEMA-co-FMA)-b-PIM copolymers.

Sample	Copolymer	Feeding ratio of DMAEMA:FMA: IM ^a CPADB (mol:mol:mol:mol)	Molar composition of DMAEMA:FMA:IM in the copolymers ^b (mol:mol:mol)	\bar{M}_n ($\times 10^4$)		PDI ^c	Yield (%)
				^1H NMR	GPC		
P0	P(DMAEMA ₁₁₈ -co-FMA ₁₇)	150:20:0:1	118:17:0	2.14	1.67	1.03	70
P1	P(DMAEMA ₁₁₈ -co-FMA ₁₇)-b-PMETAC ₂₅	150:20:30:1	118:17:25	2.66	1.73	1.04	77
P2	P(DMAEMA ₁₁₈ -co-FMA ₁₇)-b-PSBMA ₂₇	150:20:30:1	118:17:27	2.89	1.85	1.06	78
P3	P(DMAEMA ₁₁₈ -co-FMA ₁₇)-b-PSPMA ₂₇	150:20:30:1	118:17:27	2.80	1.81	1.04	78

^a IM represents the ionic monomers, i.e., METAC, SBMA or SPMA.

^b Compositions of the prepared copolymers were estimated by ^1H NMR.

^c PDI values of the prepared copolymers were obtained by GPC.

water absorption (A) was also determined as defined by the following equation [17]:

$$A (\%) = (m_1 - m_0) / m_0 \times 100 \quad (1)$$

where m_0 and m_1 represent the coating masses before and after being put into the environment with 100% RH at 25 °C for 24 h, respectively.

2.4. Hydration analyses

The water contents at different states in the coating/water binary systems were analyzed by DSC on a TA Instruments model Q2000 differential scanning calorimeter according to our previous study [19]. In brief, the samples with a certain amount of total water content were prepared by adding a given amount of deionized water and the coating/water binary systems in aluminum pans were equilibrated for 10 days in ambient conditions before measurement. The total water content (W_c), freezable water content (W_f), nonfreezable bound water content (W_{nfb}), bound water content (W_b), freezable free water content (W_{ff}) and freezable bound water content (W_{fb}) were expressed by the following equations [19]:

$$W_c = m_w / m_c \quad (2)$$

$$W_f = A_c / (334 m_c) \quad (3)$$

$$W_{nfb} = W_c - W_f \quad (4)$$

$$W_b = W_{nfb} + W_{fb} \quad (5)$$

$$W_{ff} = W_f - W_{fb} \quad (6)$$

where m_w and m_c represent the weights of the water and coating in each sample, respectively. A_c (J) was the integral area of melting peak, and 334 (J/g) was the specific heat of fusion of water [33]. W_{fb} was calculated according to the area of the symmetric peak at around -10 °C. The melting points were determined by the peak temperatures.

Raman spectra were conducted on a DXR Raman Microscope with a 532 nm laser wavelength (Thermo Fisher Scientific Co. Ltd., USA). The scan range was $500\text{--}4000\text{ cm}^{-1}$. The samples for the Raman spectra measurement containing a certain amount of deionized water were prepared by adding water into the coatings to form the coating/water binary systems, and then sealed into aluminum pans to equilibrate for several days. The total water content W_c was controlled at 3.02 mg/mg. In the case of measurements, the samples were taken out from the aluminum pans and transferred to the test bench to measure immediately. For each sample, the spectra were confirmed by at least three measurements.

Analysis of LF NMR was conducted on a Bruker Minispec mq20 spectrometer operating at a proton resonance frequency of 20 MHz at room temperature (about 20 °C). The Minispec has a $\pi/2$ pulse length of about 3.3 s. Each sample was run with 4 scans and a 2 s recycle delay

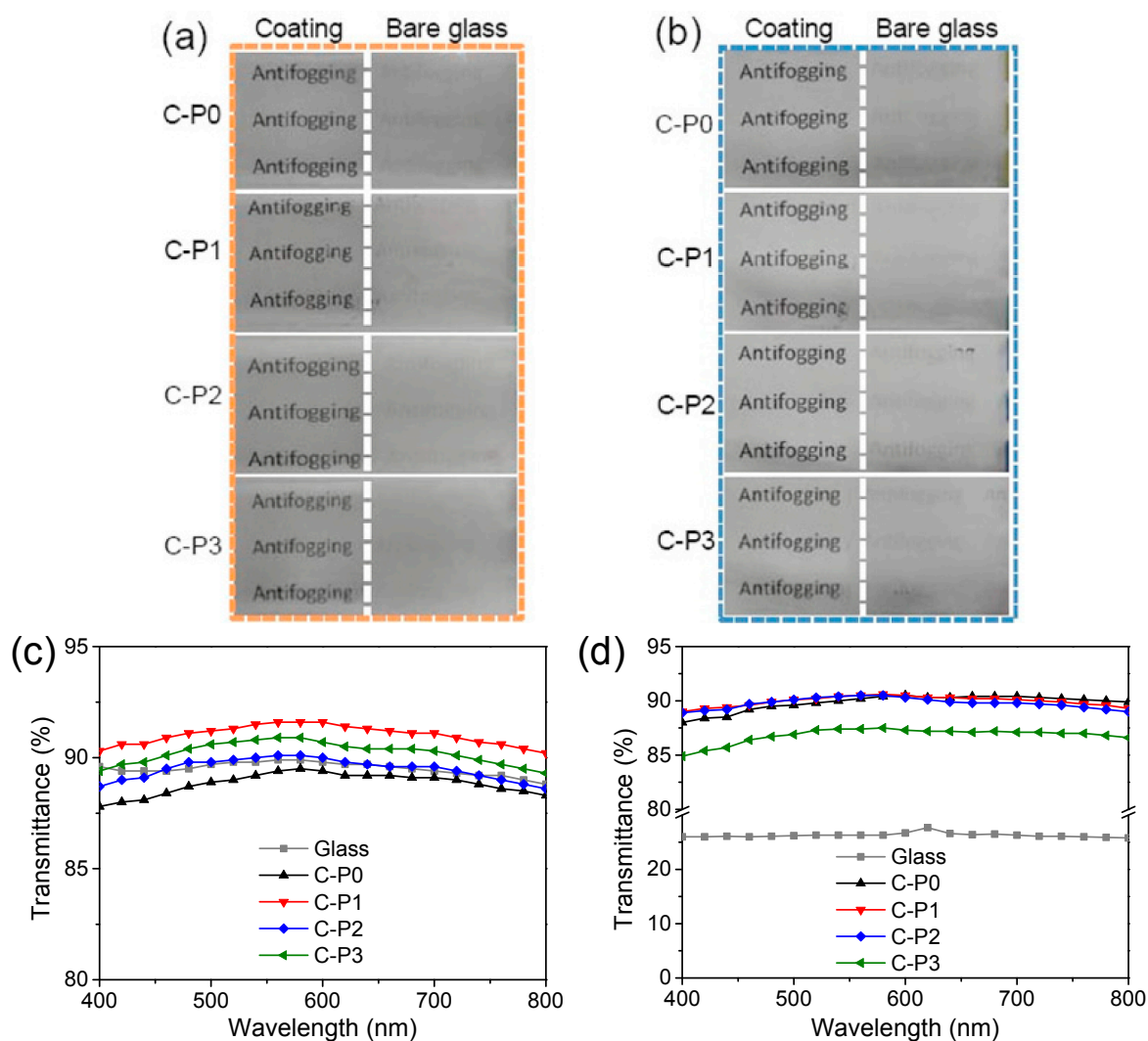


Fig. 2. Antifogging performances by hot-vapor method (a), cold-warm method (b), and the transmittance of the polyelectrolyte-based coatings before (c) and during the cold-warm antifogging test (d) in comparison with bare glass.

[34]. The samples were prepared by adding 1 mL deionized water to 333 mg copolymer in a NMR tube with a 10 mm diameter and then staying overnight to form aqueous copolymer solution. The Carr-Purcell-Meiboom-Gill (CPMG) pulse sequence was used for measuring the signal decay induced by the transverse spin-spin relaxation of protons [35,36], where a CONTIN analysis based on inverse Laplace transform was performed to extract the spin-spin relaxation time (T_2) distribution from the signal decay [37]. The apparent T_2 value for each sample was defined as the peak position of the corresponding T_2 distribution curves. Each sample was conducted three times to confirm the reliability of this method.

3. Results and discussion

Three kinds of amphiphilic coatings, C-P1, C-P2 and C-P3, were successfully prepared containing the cationic, zwitterionic and anionic copolymers P1, P2 and P3, respectively, and the coating C-P0 containing P(DMAEMA-co-FMA) was also prepared as a control. P (DMAEMA-co-FMA) was chosen as the main part of the coatings because of its good film-forming property [12–14]. Incorporation of FMA not only could regulate the hydrophilicity/hydrophobicity balance, but also could prevent the coatings from being over-swollen. The enhanced antifogging and frost-resisting performances of the prepared coatings were systematically investigated via quantitative analyses of the polymer-water interactions by DSC, Raman spectroscopy and LF NMR.

3.1. Antifogging performances

The antifogging performance of the polyelectrolyte-based coatings were investigated by hot-vapor and cold-warm methods, respectively. For the hot-vapor method, the glass substrates with both sides half coated by the coatings were put 3 cm over boiling water ($\sim 80^\circ\text{C}$ and $\sim 100\%$ RH) and a piece of paper printed with the word “Antifogging” was placed under the vessel containing hot water, photographed after remaining about 15 s. As shown in Fig. 2(a), water droplets were condensed immediately on the bare glass substrates, leading to strong light scattering and thus resulting in optical opacity. In contrast, all the coated parts maintained transparent so that the letters behind the coatings could be seen clearly, indicating excellent antifogging performance.

Furthermore, the antifogging performance of the polyelectrolyte-based coatings was investigated with the cold-warm method that first storing the samples at -20°C in a refrigerator for 30 min and then photographing immediately after exposing to the laboratory environment at a relative warm and humid conditions (15°C , 40% RH). As shown in Fig. 2(b), the relatively cold bare glass fogged immediately when taken from refrigerator to the relatively warm environment, and the image of the letters behind the glass slides became blurry severely. In comparison to the glass, almost no fog formed on the C-P0, C-P1, C-P2 and C-P3 surfaces, demonstrating the prepared polyelectrolyte-based coatings could prohibit fog formation. The remarkable antifogging properties of C-P0, C-P1, C-P2 and C-P3 could be attributed to hygroscopicity of the hydrophilic PDMAEMA, polyelectrolyte and EGDMA components in the coatings. As a result, condensed water molecules and water vapor could be absorbed into the coatings rapidly and dispersed uniformly via hydrogen-bonding interactions, while

hydrophobic FMA units could prevent excessive water molecules from entering into coatings and keep the coating surfaces dry, further leading to the enhancement of the antifogging performance.

Visible light transmittance was measured over the 400–800 nm range for the prepared coatings and bare glass (Fig. 2(c)). All the prepared coatings exhibited comparable visible light transmittance with the bare glass (about 90%), suggesting that the coating materials themselves had no effect on the transparency. To quantitatively evaluate the antifogging performance, the transmittance values from 400 to 800 nm of the prepared coatings and bare glass during the cold-warm antifogging test were also collected as shown in Fig. 2(d). According to the European Standard EN 168 [38], the antifogging performance of spectacles and goggles is evaluated by determining the time when the transmittance drops to less than 80% of the initial value. In this work, the prepared coatings C-P0, C-P1, C-P2 and C-P3 maintained the transmittance at 88.0–90.5%, 89.0–90.6%, 88.9–90.5% and 84.9–87.5%, respectively, during the cold-warm antifogging test (Fig. 2(d)), much higher than that of bare glass which dropped dramatically to 25.8–26.7%. Compared with their initial transmittance values of all about 90% (Fig. 2(c)), it could be seen that all the prepared coatings exhibited more significant antifogging properties than bare glass, though C-P3 was slightly inferior to C-P0, C-P1 and C-P2. The slightly decrease of light transmittance of C-P3 was probably due to its lower water-absorbing capacity.

As shown in Table 2, the thicknesses of C-P0, C-P1, C-P2 and C-P3 were 8.2 ± 0.3 , 8.3 ± 0.8 , 8.0 ± 0.9 and $7.7 \pm 0.3 \mu\text{m}$, respectively. The thickness of the SIPN coatings could achieve several microns, similar to the SIPN coatings with thickness of about $10 \mu\text{m}$ in our previous research [19]. It was supposed that these coatings have sufficient antifogging property. To prove this, the coatings were placed in a 100% relatively humidity environment at 25°C for 24 h and the water absorption was measured. The water absorption of C-P3 was only 26.2%, while C-P1 and C-P2 had water-absorbing capacity of about 50%, almost twice of C-P3 (Table 2). Results of the water stability (Fig. S5) indicated that all the prepared coatings exhibited good water stability, though the antifogging property was suppressed when the coatings absorbed water thoroughly. It could be seen that the antifogging properties recovered after water evaporation, indicating their long-term utilities to some extent. But, the C-P3 coating had a decrease in the transparency after immersion in water, probably caused by the conformation change of the copolymer P3 in water and the low water absorption (26.2%) of the C-P3 coating.

3.2. Surface characterizations

The surface morphology of the coating has a great influence on its light transmittance. Light scattering phenomena can be suppressed significantly by a flat coating surface [39]. Therefore, a smooth surface topography is a premise for a coating to achieve antifogging properties. The surface morphology of the prepared coatings was detected by AFM and SEM. As shown in Fig. 3(a), all the prepared coatings C-P0, C-P1, C-P2 and C-P3 presented smooth surfaces with small root-mean-square roughness (R_q) at 0.5, 1.4, 3.7 and 2.0 nm, respectively, in a measured area of $10 \times 10 \mu\text{m}^2$. The SEM images (Fig. 3(b)) indicated that the coating surfaces were relatively smooth. The smooth surfaces of all the prepared coatings would be benefit for their high transparency.

Table 2

Thickness, surface energy, surface element contents and water absorption of the polyelectrolyte-based coatings.

Sample	Thickness (μm)	Surface energy (mJ/m^2)	Surface element content (Atomic %)						Water absorption (%)
			C 1s	O 1s	N 1s	F 1s	S 2p	Cl 2p	
C-P0	8.2 ± 0.3	40.6	69.2	23.1	4.7	2.7	0.3	–	41.4
C-P1	8.3 ± 0.8	40.2	73.1	20.9	3.7	1.6	0.3	0.5	51.0
C-P2	8.0 ± 0.9	40.5	72.2	21.8	3.8	1.3	0.9	–	49.3
C-P3	7.7 ± 0.3	39.3	70.3	23.6	3.5	1.5	1.2	–	26.2

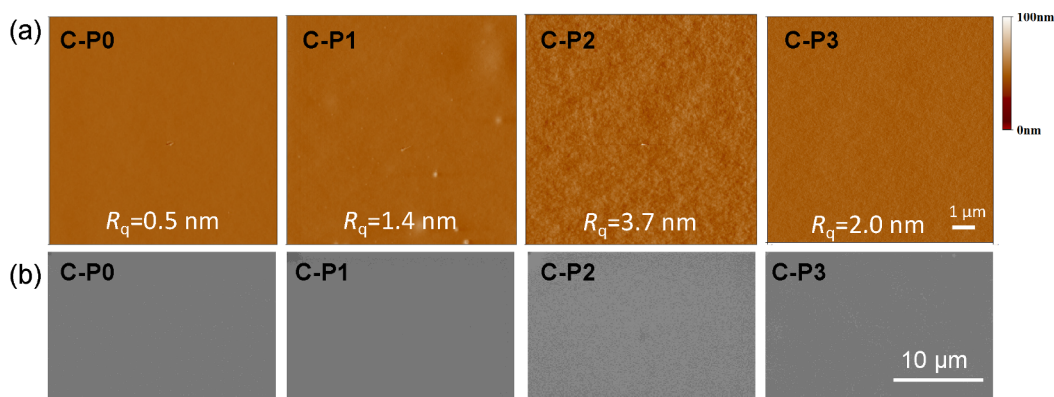


Fig. 3. AFM images (a) of the polyelectrolyte-based coatings with tapping mode over a scope of $10 \times 10 \mu\text{m}^2$, and the SEM images (b) of the prepared coatings.

To explore surface compositions of the prepared coatings, ATR-FTIR and XPS measurements were conducted. It can be seen from the ATR-FTIR spectra in Fig. 4(a), that the peaks at 2816 and 2766 cm^{-1} belonged to C–H vibration of $-\text{N}(\text{CH}_3)_2$ in PDMAEMA, while the signals at 1722 and 1270 cm^{-1} were attributed to characteristic absorptions of C=O and C–N, respectively. Furthermore, the peak at 660 cm^{-1} was related to C–F bending vibration of FMA in all the C-P0, C-P1, C-P2 and C-P3 coatings. The absorption peak at 960 cm^{-1} was corresponded to C–H vibration of quaternary in C-P1 and C-P2, and the characteristic absorption peak at 1036 cm^{-1} was corresponding to S=O symmetric stretching vibration of $-\text{SO}_3$ in C-P2 and C-P3. The results of ATR-FTIR suggested that all the three kinds of the prepared copolymers could be detected on the surface of the corresponding coatings.

The XPS results are presented in Fig. 4(b,c) and Table 2. As expected, the representative binding energy peaks of C 1s, O 1s and N 1s appeared at 289, 534 and 400 eV, respectively (Fig. 4(b)). For each sample, the peaks at 688 eV were assigned to F 1s coming from FMA units in the copolymer. As shown in Fig. 4(c), it could be observed that S 2p were existent in C-P2 and C-P3 and almost absent in C-P0 and C-P1, one more time indicating different kinds of P(DMAEMA-co-FMA)-b-PIM copolymers were detectable on the coating surfaces. It was noted that small peaks of C-P0 and C-P1 in S 2p high-resolution spectra were attributed to the chain transfer agent CPADB at the end of macromolecular chains. The elemental contents on the prepared coating surfaces are shown in Table 2, suggesting that each coating had comparable C 1s, O 1s and N 1s contents. Because of the random copolymerization of DMAEMA and FMA with short fluorinated side groups in the prepared copolymers, the F contents on all the coating surfaces were lower than that of bulk F contents (about 2.5%), implying that FMA units could possibly disperse evenly in the coating and on the coating surfaces.

3.3. Wettability

To elucidate the correlation between the antifogging properties and surface wettability of the prepared coatings, time-dependent WCA values on these surfaces were recorded over a 300 s period under the ambient conditions. Effect of the EGDMA content on the wettability of the coating surfaces was investigated and the result shown in Fig. S6 indicated that variation of the WCA values for all the coatings was slight when the EGDMA content increased from 2 to 10 wt%. It was assumed that the EGDMA content had a little effect on the wettability of the polyelectrolyte-based coatings when EGDMA content was 2, 5, and 10 wt%. Then, the WCA evolution of the polyelectrolyte-based coatings (EGDMA content was 10 wt%) was performed and shown in Fig. 5(a), C-P1, C-P2 and C-P3 exhibited almost similar initial WCA values around 68° with that of C-P0, suggesting that these effective antifogging coatings were not superhydrophilic. For C-P1, the initial WCA value was $67.1 \pm 3.1^\circ$, followed by a rapid decrease to $34.3 \pm 7.1^\circ$ in 300 s

because of the polymer-water interactions, much more quickly than the variation of WCA value on the bare glass due to water evaporation. Meanwhile, the WCA value of C-P2 dropped from its initial value of $66.7 \pm 1.3^\circ$ to $45.4 \pm 0.6^\circ$ over 300 s. The decrease of WCAs for C-P1 and C-P2 were more rapidly than C-P0 during the 300 s time interval because of the high hydrophilicity and hygroscopicity of polyelectrolytes. This time-dependent behavior was mainly due to transient surface reconstruction, in which the hydrophilic components could reorganize to the coating surfaces in response to water droplets [40,41]. In this case, the coatings could absorb water molecules more quickly, thus enhancing antifogging performance. It was noted that the decrease of WCA values of C-P2 and C-P3 were less than that of C-P1, especially for C-P3, which variation trend was almost the same as C-P0. The surface energy of the prepared coatings was also measured by the OWK method. As shown in Table 2, the C-P0, C-P1, C-P2 and C-P3 coatings showed similar surface energy of 40.6, 40.2, 40.5 and 39.3 mJ/m^2 , respectively.

When water molecules are absorbed into the coatings, whether it can be spread evenly in the coatings within a short time is also of importance for antifogging performance. As shown in Fig. 5(b), the

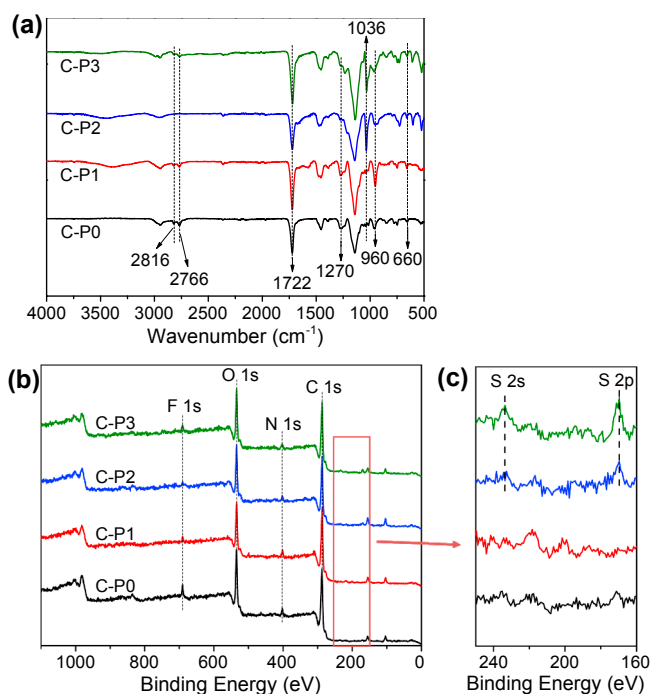


Fig. 4. ATR-FTIR (a), XPS survey (b) and S 2p high-resolution spectra (c) of the polyelectrolyte-based coatings.

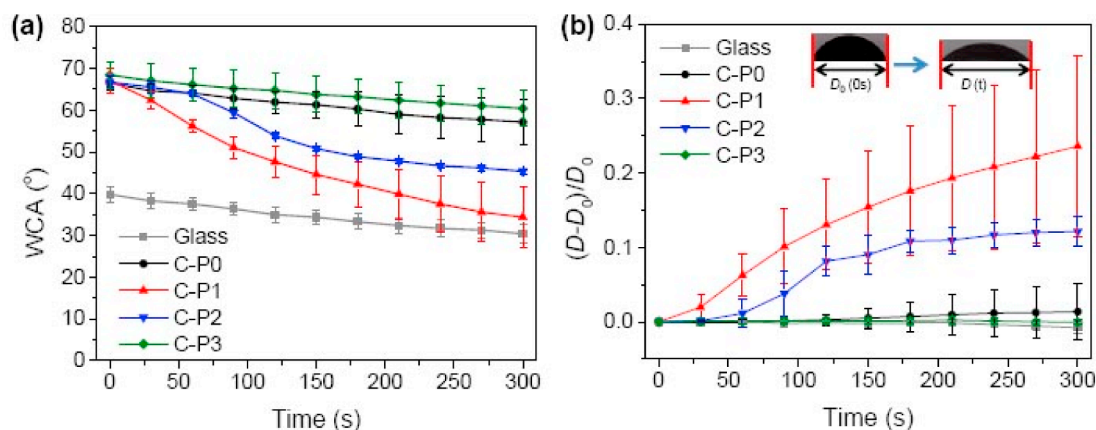


Fig. 5. Evolution of the water contact angle (WCA) (a) and the water droplet diameter (b) on the prepared coatings with the time in 300 s, where D_0 is the original diameter ($t = 0$ s) of the water droplet, and D is the water droplet diameter at a given time during the experiment.

diameter evolution of water droplets on the coating surfaces were recorded. The droplets diameter on C-P1 and C-P2 increased by 23% and 12% in 300 s, respectively, indicating that condensed water droplets could spread on the surfaces and disperse into the coatings rapidly. Thus, the antifogging properties could be attributed to excellent hydrophilicity of the hydrophilic components in the cross-linked coatings. However, the droplet diameter on C-P0 and C-P3 surfaces as well as bare glass surface nearly remained unchanged over the experiment process, implying the C-P0 and C-P3 had an inferior water-absorbing capacity. This result was in accordance with the water absorption test (Table 2). Obviously, C-P1 and C-P2 exhibited superior antifogging behavior. Notably even C-P0 and C-P3 coating surfaces showed nearly same wettability, while C-P0 exhibited better antifogging properties than C-P3.

3.4. Frost-resisting performances

The usual testing method of frost-resisting properties of coatings was the cold-fog test which held the sample at very low initial temperature and then exposed to room temperature and high humidity [11,12,14,24]. However, this method could not reflect the actual frosting situation to some extent. Thus, it is essential to evaluate condensation frosting state of coatings at subzero temperature and high humidity. In our experiment, the samples were placed on a cooling stage horizontally at room temperature then cooled to -5 °C and held on at this temperature. The frost formation on the prepared coatings and bare glass with time evolution were presented in Fig. 6. The time was recorded when the stage temperature reached -5 °C. During the temperature decrease process, condensation was observed on the bare glass surface, causing fog formation. When the stage cooled to -5 °C, the bare glass surface was already covered by small water droplets and became opaque in 2 min. It can be seen that after 18 min of freezing, the bare glass surface was covered by frost which became thicker as time went on. However, for all the prepared coatings, there was no frost formation on the surfaces within 18 min, indicating water molecules could be absorbed into the coatings. C-P2 had a slight crack at the edge of the coating after 18 min of freezing, probably due to their less water stability under low temperature and high humidity conditions. C-P1 exhibited comparable frost-resisting performance with C-P2 after 30 min of freezing. Then the frost began to form on the outer edge of C-P1 due to the edge effect, specifically geometric singularity and lower energy barrier for heterogeneous nucleation [22]. C-P0 and C-P3 showed remarkable frost-resisting properties as long as 35 min, though their surfaces were covered by frost as the time extended to 45 min. The frost-resisting performance of coatings could be attributed to balanced hydrophilicity and hydrophobicity. Water molecules could form

nonfreezable bound water in hydrophilic polymers which does not crystallize even at a temperature as low as -100 °C [42]. The non-freezable bound water could decrease the freezing point of water, which plays an important role in preventing frost formation. For C-P1 and C-P2, it was probably because of overwhelming water absorbed into the coatings. The existence of free water in the coatings made the frost-resisting property invalid. On the other hand, C-P0 and C-P3 showed lower water-absorbing capacity than C-P1 and C-P2, resulting in less free water existence in C-P0 and C-P3, making them exhibit better frost-resisting performance.

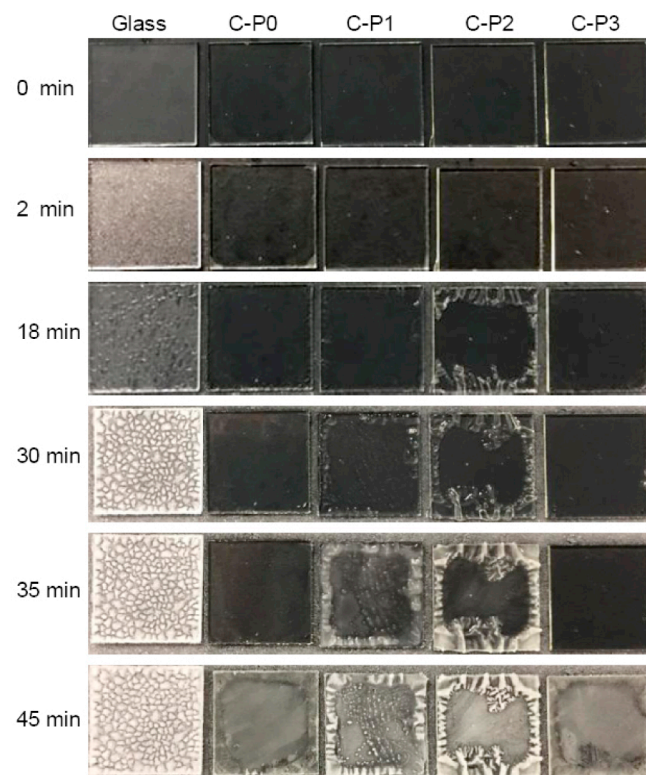


Fig. 6. Optical images of the frost formation on the prepared coatings and bare glass with time. The samples in 1×1 cm² were placed on a cooling stage horizontally that was controlled at -5 °C, relative humidity of 50%. The time was recorded when the stage temperature cooled to -5 °C from room temperature at a rate of 2 °C/min.

3.5. Analyses of polymer-water interactions

DSC, Raman spectroscopy and LF NMR were used to quantitatively characterize the polymer-water interactions for the further analyses of the hydration impact on the antifogging/frost-resisting performances of the amphiphilic coatings. DSC was used to analyze the water contents at different states in the coating/water binary systems. The DSC curves of the binary systems with the total water content (W_c) of ca. 0.55 mg/mg in the heating process at a rate of 10 °C/min are shown in Fig. 7. It can be seen that two water melting endotherms were observed in the heating curves, one at ca. 0 °C, corresponding to the melting point of freezable free water (W_{ff}), and the other towards lower temperature assigned to the freezable bound water (W_{fb}). W_{ff} and W_{fb} were calculated by peak decomposition via Origin 8.0 software. The nonfreezable bound water content (W_{nfb}) was obtained from the difference between the total water content and the freezable water content (W_f).

The water contents at different states analyzed by DSC are summarized in Table 3. In C-P1 coating/water binary system, the non-freezable bound water content W_{nfb} and the total bound water content W_b were 0.40 and 0.47 mg/mg, respectively, which were the highest among all the coating/water binary systems. It is worth to mention that the threshold of nonfreezable bound water for a given polymer is a characteristic value, which was related to the ability of water molecules to interact with polar groups in the polymers [42]. Therefore, the polymer-water interactions of cationic C-P1 would be stronger than that of other samples. The W_{nfb} in C-P0 coating/water binary system was 0.29 mg/mg, indicating lower polymer-water interactions than those of others due to the absence of ionic monomers. C-P2 and C-P3 coating/water binary systems had similar W_b , and in comparison with anionic C-P3, a little higher W_{nfb} formed in the C-P2 binary system, implying the formation of stronger hydrogen bonds in zwitterionic C-P2 coating/water binary system.

Although hydrogen bonds are virtual and invisible, Raman spectroscopy had been employed to study the hydration behaviors. For instance, it could be used to analyze the OH stretching mode of water molecules near the glass particles surface with different hydrophobicity both immersed in water and clathrate hydrates [43]. In this study, Raman spectroscopy was used to detect the presence of hydrogen bonds and their relative intensity. The samples containing a certain amount of deionized water ($W_c = 3.02$ mg/mg) were prepared by adding water into the coatings to form binary systems. As shown in Fig. 8(a), Raman bands of C-P1, C-P2 and C-P3 centered near 3230 and 3450 cm^{-1} were assigned to hydrogen bonds, which corresponded to vibrations of strong hydrogen bonds in tetrahedral coordination and weak hydrogen bonds in an incomplete tetrahedral structure, respectively [44]. In other words, the two bands were also known as the ‘ice-like’ and ‘liquid-like’ modes [45]. Furthermore, the relative intensity ratio of the two bands (I_{3230}/I_{3450}) could be used to estimate the ratio of tetrahedrally coordinated strong hydrogen bonds to that of weak hydrogen bonds [43]. The I_{3230}/I_{3450} ratio in C-P1 and C-P2 coating/water binary systems was 1.17 and 1.18, respectively, both higher than 0.80 in C-P3 coating/water binary system, indicating that relative high number of hydrogen bonds in ice-like mode were formed in C-P1 and C-P2 coating/water binary systems. As a contrast, no obvious hydrogen-bonding peaks were observed in C-P0, suggesting that the incorporation of polyelectrolytes could enhance hydrogen-bonding interactions between coatings and water molecules. The results were basically consistent with the results obtained in the above DSC results, where the strongest hydrogen bonds formed in C-P1 coating/water binary system with the highest non-freezable bound water content.

LF NMR is also powerful for characterizing polymer-water interactions by measuring transverse spin-spin relaxation time (T_2) which can provide information about proton mobility in aqueous solution [46]. To further reveal the differences of synthesized copolymers in hydration behavior, the CPMG measurement was adopted to detect T_2 as well as the distribution of water molecules in aqueous copolymer solutions.

Fig. 8(b) showed relaxation time distribution curves of the P0, P1, P2 and P3 aqueous solutions and deionized water, obtained from the CONTIN analysis on the CPMG decay curves. It can be seen that the deionized water exhibited one peak ($T_2 = 2017$ ms) as expected [46,47]. For P0 aqueous solution, a broad peak with a lower T_2 (1720 ms) was observed, indicating that the water molecules moved slowly due to interactions between P0 copolymer and water molecules. The wide T_2 distribution curve of P0 was probably caused by the random structure in P0, where the hydrophilic DMAEMA and hydrophobic FMA were randomly copolymerized. Compared with P0 aqueous solution, P1, P2 and P3 aqueous solutions showed lower T_2 values, suggesting that the motion of water molecules was more restricted in the aqueous solution. It was attributed to the formation of hydrogen bonds between the polyelectrolyte-based copolymer and water molecules, which was consistent with the results obtained from Raman spectroscopy, where hydrogen bonds were formed in P1, P2, P3 coating/water binary systems. Therefore, it could be concluded that incorporation of polyelectrolyte could improve polymer-water interactions for improving antifogging and frost-resisting properties.

Among polyelectrolyte containing copolymers, P1 exhibited the lowest T_2 value (764 ms), while P3 showed the highest one (1641 ms). It was reported that the contribution of bound water could cause the decrease in T_2 compared with pure water (free water) [47]. The more bound water content formed, the more decrease in T_2 values. Therefore, combined with the above DSC and Raman spectroscopy results, it could be known that the more bound water formed when P1 interacted with water molecules via stronger hydrogen bonds. In the contrary, the hydrogen-bonding interactions with water molecules were moderate in P2, and P3 had the weakest interactions with water molecules, leading to the relative longer T_2 values. It was probably due to the electrostatic interactions between DMAEMA and SBMA in P2 or SPMA units in P3, and these electrostatic interactions could possibly affect the hydrogen-bonding interactions between copolymers and water molecules. Moreover, two peaks were observed for P3 aqueous solution. The peak with a lower T_2 value (336 ms) could be attributed to the protons of P3

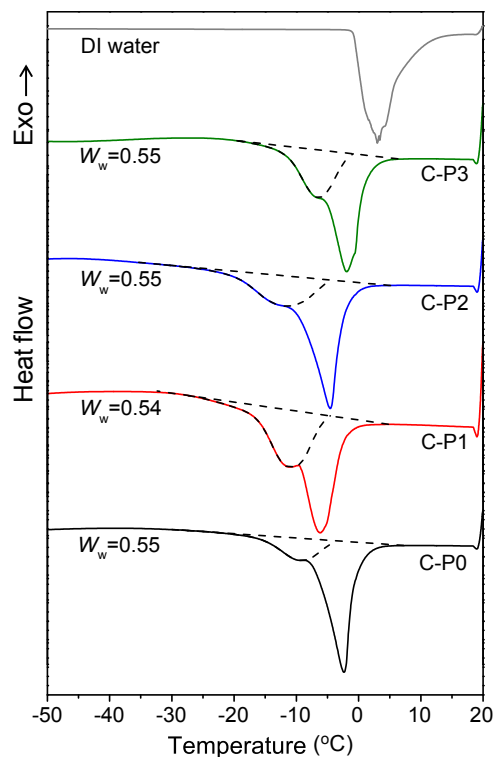


Fig. 7. DSC heating curves of the prepared coatings with $W_c \approx 0.55$ mg/mg as well as deionized water at a heating rate of 10 °C/min.

Table 3
Water contents (mg/mg) at different states in the coating/water binary systems.

Sample	W_c	W_f		W_{nfb}	W_b
		W_{ff}	W_{fb}		
C-P0	0.55	0.20	0.06	0.29	0.35
C-P1	0.54	0.07	0.07	0.40	0.47
C-P2	0.55	0.12	0.07	0.36	0.43
C-P3	0.55	0.12	0.08	0.35	0.43

copolymer [46].

To verify this idea, the copolymer morphology in the aqueous solution was detected by AFM and TEM as shown in Fig. S4. From the AFM and TEM images, it can be seen that the P0 copolymer could dissolve well in the water, whereas there were aggregates in the P1, P2 and P3 copolymer solutions. P3 could form large aggregates with diameter of 100–500 nm, larger than P1 and P2 copolymers, that could be due to the electrostatic interactions between DMAEMA and SPMA units in P3. Thus, the hydrogen-bonding interactions between P3 and water could be weakened so that the C-P3 coating had a relatively reduced hydrophilicity, which was consistent with WCA, DSC and Raman spectra results.

From the above analyses of DSC, Raman spectroscopy and LF NMR, it was suggested that the amphiphilic coatings containing cationic, zwitterionic and anionic units exhibited optimum antifogging and frost-resisting properties owing to favorable water-absorbing capacity and balanced hydrophilicity/hydrophobicity. As illustrated in Fig. 9, hydrogen bonds between copolymers and water molecules could be easily formed in the cationic coating C-P1, making the condensed water droplets rapidly absorbed into the coating. Due to electrostatic interactions between zwitterionic polyelectrolyte and DMAEMA, the formation of hydrogen bonds with water molecules was restricted to a certain extent in C-P2. For the anionic coating C-P3, hydrogen-bonding interactions was greatly weakened by the existence of strong

intermolecular and intramolecular electrostatic interactions between SPMA and DMAEMA units, that was suitable for frost-resisting because it had a low water absorption ability that could delay frost formation under high humidity and low temperature.

4. Conclusions

In summary, we developed three kinds of amphiphilic coatings by casting the copolymer solutions of P(DMAEMA-co-FMA)-b-PMETAC, P(DMAEMA-co-FMA)-b-PSBMA or P(DMAEMA-co-FMA)-b-PSPMA with EGDMA via subsequent UV-curing. The resulting cationic and zwitterionic coatings containing METAC and SBMA, respectively, exhibited excellent antifogging performances attributed to stronger polymer-water interactions, and the anionic coating showed remarkable frost-resisting properties. The strongest polymer-water interactions in the cationic C-P1 coating were proved by the quantitative analyses of DSC, Raman spectra and LF NMR relaxation time T_2 . DSC results showed that 0.47 mg/mg bound water formed in C-P1 coating/water binary system, whereas there was 0.43 mg/mg formed in zwitterionic and anionic binary systems. The relative intensity ratio I_{3230}/I_{3450} in the Raman spectra were 1.17 and 0.8 for the C-P1 and C-P3 binary systems, respectively, and the shortest T_2 of 764 ms for P1 aqueous solution from LF NMR. Furthermore, balanced hydrophilicity/hydrophobicity was necessary for prohibiting frost formation when the temperature was subzero. Since the electrostatic interactions between anionic SPMA and cationic DMAEMA weakened the polymer-water interactions, the anionic C-P3 coating exhibited the lowest water absorption of 26.2%, endowing its excellent frost-resisting properties. The antifogging and frost-resisting properties of the zwitterionic C-P2 coating were moderate between the cationic C-P1 and anionic C-P3 coatings. It was suggested that the polyelectrolyte-based coatings with high antifogging and frost-resisting behaviors could be used in specific conditions.

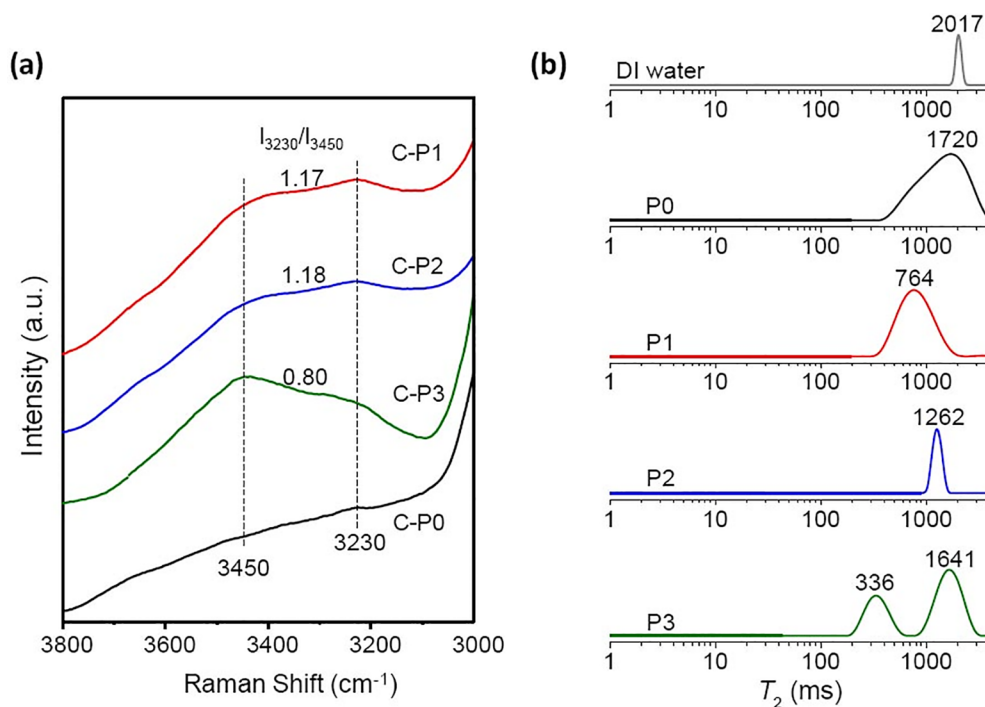


Fig. 8. Raman spectra (a) of the coating/water binary systems when the total water content was 3.02 mg/mg and relaxation time (T_2) distribution curves (b) of the synthesized P0, P1, P2 and P3 copolymers in the aqueous solution as well as deionized water.

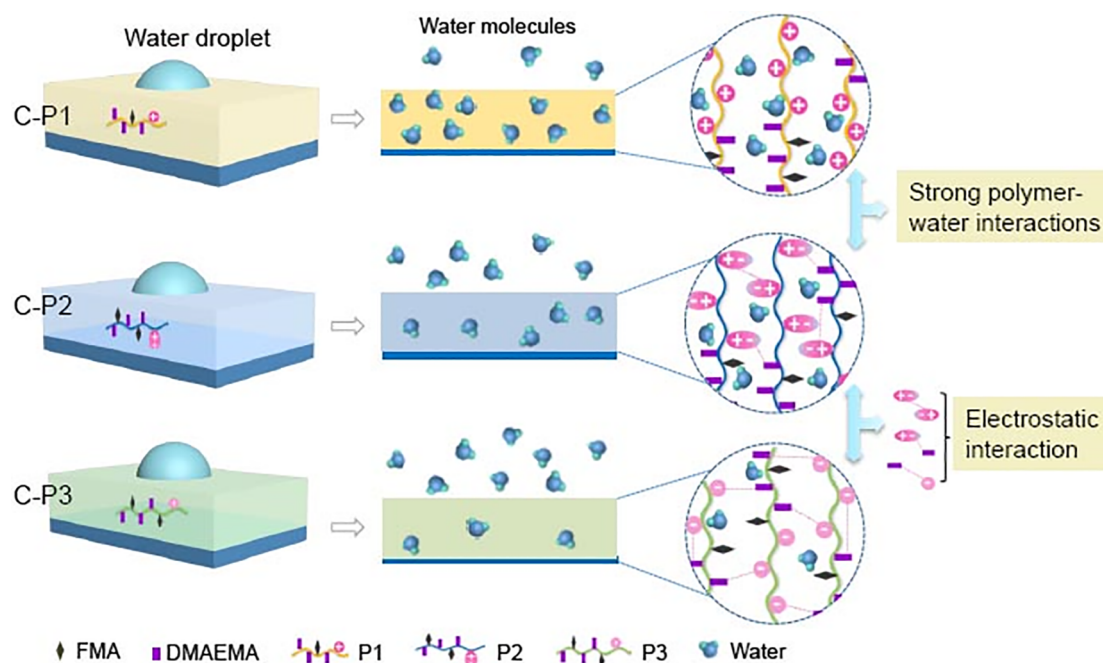


Fig. 9. Illustration of the polymer-water interactions in the polyelectrolyte-based C-P1, C-P2 and C-P3 coatings containing cationic, zwitterionic and anionic units, respectively.

Conflicts of interest

There are no conflicts to declare.

Acknowledgments

This work is financially supported by the National Natural Science Foundation of China (No. 51603143) and the Natural Science Foundation of Tianjin, China (No. 18JCQNJC03800).

Appendix A. Supplementary data

Supplementary data to this article can be found online at <https://doi.org/10.1016/j.cej.2018.09.177>.

References

- Z. Han, X. Feng, Z. Guo, S. Niu, L. Ren, Flourishing bioinspired antifogging materials with superwettability: progresses and challenges, *Adv. Mater.* 1704652 (2018).
- J. Zhao, L. Song, W.H. Ming, Antifogging and frost-resisting polymeric surfaces, *Advances in Polymer Science*, Springer, Berlin, Heidelberg, 2017, pp. 1–30.
- T. Mouterde, G. Lehoucq, S. Xavier, A. Checco, C.T. Black, A. Rahman, T. Midavaine, C. Clanet, D. Quéré, Antifogging abilities of model nanotextures, *Nat. Mater.* 16 (2017) 658–663.
- C. Liu, J. Ju, Y. Zheng, L. Jiang, Asymmetric ratchet effect for directional transport of fog drops on static and dynamic butterfly wings, *ACS Nano* 8 (2014) 1321–1329.
- M. Choi, L. Xiangde, J. Park, D. Choi, J. Heo, M. Chang, C. Lee, J. Hong, Superhydrophilic coatings with intricate nanostructure based on biotic materials for antifogging and antibiofouling applications, *Chem. Eng. J.* 309 (2017) 463–470.
- Z. Han, Z. Mu, B. Li, Z. Wang, J. Zhang, S. Niu, L. Ren, Active antifogging property of monolayer SiO₂ film with bioinspired multiscale hierarchical pagoda structures, *ACS Nano* 10 (2016) 8591–8602.
- T.P. Allred, J.A. Weibel, S.V. Garimella, A wettability metric for characterization of capillary flow on textured superhydrophilic surfaces, *Langmuir* 33 (2017) 7847–7853.
- B. Dudem, L.K. Bharat, J.W. Leem, D.H. Kim, J.S. Yu, Hierarchical Ag/TiO₂/Si forest-like nano/micro-architectures as antireflective, plasmonic photocatalytic, and self-cleaning coatings, *ACS Sustain. Chem. Eng.* 6 (2017) 1580–1591.
- M. Wen, L. Wang, M. Zhang, L. Jiang, Y. Zheng, Antifogging and icing-delay properties of composite micro-and nanostructured surfaces, *ACS Appl. Mater. Interfaces* 6 (2014) 3963–3968.
- M. Zhang, L. Wang, S. Feng, Y. Zheng, A strategy of antifogging: air-trapped hollow microsphere nanocomposites, *Chem. Mater.* 29 (2017) 2899–2905.
- Y. Wang, T. Li, S. Li, J. Sun, Antifogging and frost-resisting polyelectrolyte coatings capable of healing scratches and restoring transparency, *Chem. Mater.* 27 (2015) 8058–8065.
- J. Zhao, A. Meyer, L. Ma, W.H. Ming, Acrylic coatings with surprising antifogging and frost-resisting properties, *Chem. Commun.* 49 (2013) 11764–11766.
- J. Zhao, L. Ma, W. Millians, T. Wu, W.H. Ming, Dual-functional antifogging/anti-microbial polymer coating, *ACS Appl. Mater. Interfaces* 8 (2016) 8737–8742.
- J. Zhao, A. Meyer, L. Ma, X. Wang, W.H. Ming, Terpolymer-based SIPN coating with excellent antifogging and frost-resisting properties, *RSC Adv.* 5 (2015) 102560–102566.
- H. Lee, J.B. Gilbert, F.E. Angile, R. Yang, D. Lee, M.F. Rubner, R.E. Cohen, Design and fabrication of zwitter-wettable nanostructured films, *ACS Appl. Mater. Interfaces* 7 (2015) 1004–1011.
- J.A. Howarter, J.P. Youngblood, Self-cleaning and anti-fog surfaces via stimuli-responsive polymer brushes, *Adv. Mater.* 19 (2007) 3838–3843.
- F. Xu, X. Li, Y. Li, J. Sun, Oil-repellent antifogging films with water-enabled functional and structural healing ability, *ACS Appl. Mater. Interfaces* 9 (2017) 27955–27963.
- H. Guo, T. Xu, J. Zhang, W. Zhao, J. Zhang, C. Lin, L. Zhang, A multifunctional anti-fog, antibacterial, and self-cleaning surface coating based on poly(NVP-co-MA), *Chem. Eng. J.* 351 (2018) 409–417.
- C. Li, X. Li, C. Tao, L. Ren, Y. Zhao, S. Bai, X. Yuan, Amphiphilic antifogging/anti-icing coatings containing POSS-PDMAEMA-*b*-PSBMA, *ACS Appl. Mater. Interfaces* 9 (2017) 22959–22969.
- H. Lee, M.L. Alcaraz, M.F. Rubner, R.E. Cohen, Zwitter-wettability and antifogging coatings with frost-resisting capabilities, *ACS Nano* 7 (2013) 2172–2185.
- F. Wang, C. Liang, X. Zhang, Research of anti-frosting technology in refrigeration and air conditioning fields: a review, *Renew. Sust. Energ. Rev.* 81 (2018) 707–722.
- Y. Zhang, M.R. Klittich, M. Gao, A. Dhinojwala, Delaying frost formation by controlling surface chemistry of carbon nanotube-coated steel surfaces, *ACS Appl. Mater. Interfaces* 9 (2017) 6512–6519.
- W. Zhang, S. Wang, Z. Xiao, X. Yu, C. Liang, Y. Zhang, Frosting behavior of superhydrophobic nanoarrays under ultralow temperature, *Langmuir* 33 (2017) 8891–8898.
- M. Ezzat, C. Huang, Zwitterionic polymer brush coatings with excellent anti-fog and anti-frost properties, *RSC Adv.* 6 (2016) 61695–61702.
- Z. He, L. Zheng, Z. Liu, S. Jin, C. Li, J. Wang, Inhibition of heterogeneous ice nucleation by bioinspired coatings of polyampholytes, *ACS Appl. Mater. Interfaces* 9 (2017) 30092–30099.
- H. Guo, P. Sun, Y. Liang, Y. Ma, Z. Qin, S. Cui, In-situ fabrication of polyelectrolyte-CSH superhydrophilic coatings via layer-by-layer assembly, *Chem. Eng. J.* 253 (2014) 198–206.
- Z. He, W. Xie, Z. Liu, G. Liu, Z. Wang, Y. Gao, J. Wang, Tuning ice nucleation with counterions on polyelectrolyte brush surfaces, *Sci. Adv.* 2 (2016) e1600345.
- Y. Jin, Z. He, Q. Guo, J. Wang, Control of ice propagation via polyelectrolyte multilayer coatings, *Angew. Chem. Int. Ed.* 56 (2017) 11436–11439.
- Y. Fu, J. Jiang, Q. Zhang, X. Zhan, F. Chen, Robust liquid-repellent coatings based on polymer nanoparticles with excellent self-cleaning and antibacterial performances, *J. Mater. Chem. A* 5 (2017) 275–284.
- C. Tao, S. Bai, X. Li, C. Li, L. Ren, Y. Zhao, X. Yuan, Formation of zwitterionic coatings with an aqueous lubricating layer for antifogging/anti-icing applications, *Prog. Org. Coat.* 115 (2018) 56–64.

- [31] P. Pallavicini, A. Taglietti, G. Dacarro, Y.A. Diaz-Fernandez, M. Galli, P. Grisoli, M. Patrini, G.S.D. Magistris, R. Zanoni, Self-assembled monolayers of silver nanoparticles firmly grafted on glass surfaces: low Ag⁺ release for an efficient anti-bacterial activity, *J. Colloid Interface Sci.* 350 (2010) 110–116.
- [32] H.X. Fang, S.X. Zhou, L.M. Wu, Microphase separation behavior on the surfaces of PEG-MDI-PDMS multiblock copolymer coatings, *Appl. Surf. Sci.* 253 (2006) 2978–2983.
- [33] U. Weise, T. Maloney, H. Paulapuro, Quantification of water in different states of interaction with wood pulp fibres, *Cellulose* 3 (1996) 189–202.
- [34] R. Zhang, S. Yu, S. Chen, Q. Wu, T. Chen, P. Sun, B. Li, D. Ding, Reversible cross-linking, microdomain structure, and heterogeneous dynamics in thermally reversible cross-linked polyurethane as revealed by solid-state NMR, *J. Phys. Chem. B* 118 (2014) 1126–1137.
- [35] H.Y. Carr, E.M. Purcell, Effects of diffusion on free precession in nuclear magnetic resonance experiments, *Phys. Rev.* 94 (1954) 630–638.
- [36] S. Meiboom, D. Gill, Modified spin-echo method for measuring nuclear relaxation times, *Rev. Sci. Instrum.* 29 (1958) 688–691.
- [37] S.W. Provencher, CONTIN: a general purpose constrained regularization program for inverting noisy linear algebraic and integral equations, *Comput. Phys. Commun.* 27 (1982) 229–242.
- [38] BS EN 168, Personal eye-protection – non-optical test methods, British Standards Institute, London, 2002.
- [39] K. Manabe, C. Tanaka, Y. Moriyama, M. Tenjimbayashi, C. Nakamura, Y. Tokura, T. Matsubayashi, K. Kyung, S. Shiratori, Chitin nanofibers extracted from crab shells in broadband visible antireflection coatings with controlling layer-by-layer deposition and the application for durable antifog surfaces, *ACS Appl. Mater. Interfaces* 8 (2016) 31951–31958.
- [40] A. Horinouchi, H. Atarashi, Y. Fujii, K. Tanaka, Dynamics of water-induced surface reorganization in poly(methyl methacrylate) films, *Macromolecules* 45 (2012) 4638–4642.
- [41] S. Farris, L. Introzzi, P. Biagioni, T. Holz, A. Schiraldi, L. Piergiorganni, Wetting of biopolymer coatings: contact angle kinetics and image analysis investigation, *Langmuir* 27 (2011) 7563–7574.
- [42] Z. Ping, Q.T. Nguyen, S. Chen, J. Zhou, Y. Ding, States of water in different hydrophilic polymers-DSC and FTIR studies, *Polymer* 42 (2001) 8461–8467.
- [43] H. Li, P. Stanwix, Z. Aman, M. Johns, E. May, L. Wang, Raman spectroscopic studies of clathrate hydrate formation in the presence of hydrophobized particles, *J. Phys. Chem. A* 120 (2016) 417–424.
- [44] V.S. Marinov, Z.S. Nickolov, H. Matsuura, Raman spectroscopic study of water structure in aqueous nonionic surfactant solutions, *J. Phys. Chem. B* 105 (2001) 9953–9959.
- [45] J. Nakahara, Y. Shigesato, A. Higashi, T. Hondoh, C.C. Langway Jr, Raman spectra of natural clathrates in deep ice cores, *Philos. Mag. B* 57 (1988) 421–430.
- [46] J. Chen, X. Gong, C. Zeng, Y. Wang, G. Zhang, Mechanical insight into resistance of betaine to urea-induced protein denaturation, *J. Phys. Chem. B* 120 (2016) 12327–12333.
- [47] Y. Chi, S. Xu, X. Xu, Y. Cao, J. Dong, Studies of relationship between polymer structure and hydration environment in amphiphilic polytartaramides, *J. Polym. Sci. Pol. Phys.* 55 (2017) 138–145.